Cite this article
Huber JAJ, Ekevad M, Girhammar UA and Berg S (2020)
Finite element analysis of alternative load paths in a platform-framed CLT building.
Proceedings of the Institution of Civil Engineers – Structures and Buildings **173(5)**: 379–390,
https://doi.org/10.1680/jstbu.19.00136

Research Article
Paper 1900136
Received 30/06/2019;
Accepted 26/11/2019;
Published online 27/01/2020

Keywords: computational mechanics/ safety & hazards/timber structures

Structures and Buildings

ice Publishing

Finite element analysis of alternative load paths in a platform-framed CLT building

1 Johannes A. J. Huber MSc
PhD student, Division of Wood Science and Engineering, Luleå University of Technology, Skellefteå, Sweden (corresponding author: johannes.huber@ltu.se) (Orcid:0000-0001-9196-0370)

2 Mats Ekevad PhD
Professor, Division of Wood Science and Engineering, Luleå University of Technology, Skellefteå, Sweden (Orcid:0000-0002-0145-080X)

3 Ulf Arne Girhammar PhD
Professor, Division of Wood Science and Engineering, Luleå University of Technology, Skellefteå, Sweden (Orcid:0000-0002-0336-6433)

4 Sven Berg PhD
Senior Lecturer, Division of Wood Science and Engineering, Luleå University of Technology, Skellefteå, Sweden (Orcid:0000-0002-4686-4010)




Multi-storey cross-laminated timber (CLT) buildings are a comparatively recent construction type. Knowledge concerning the performance of CLT buildings regarding the prevention of disproportionate collapse after unforeseeable events (e.g. accidents or acts of terrorism) is not as refined as that for concrete and steel buildings. In particular, alternative load paths (ALPs) after the removal of a wall panel in platform-framed variants have not yet been studied in detail. The goal of this work was therefore to study ALPs in CLT buildings. An eight-storey bay of an existing building was evaluated by conducting a non-linear static pushdown analysis in a finite element analysis on three representative storeys. The analyses accounted for single fastener behaviour, timber crushing, friction, brittle failure and large deformations. The force–deformation behaviours elicited under the pushdown analyses were subsequently inserted in a simplified dynamic model to evaluate the transient response of the entire bay. Four ALPs were identified in this case – shear resistance in the floor panels, arching action of the walls, catenary action in the floor panels and hanging action from the roof. The dynamic analysis did not show a collapse, unless the inter-compartment stiffness was significantly reduced. The resistance mechanisms are described in this paper, which may provide information for improved building design.

Notation

A	total horizontal cross sectional surface of four wall panels (m^2)
C	disproportionate collapse
D	local damage
d	nominal screw diameter (mm)
E	unexpected event
$F_{ax,max}$	axial screw strength (N)
F_i	force along the ith degree of freedom (DoF) (kN)
$F_{lat,y}$	yield point of lateral screw loading (N)
F_{max}	maximum or ultimate force (kN)
$F_{R,a}$ to $F_{R,f}$	Johansen yield strengths (N)
F_y	yield force (kN)
$f_{c,k}$	characteristic compressive strength (MPa)
$f_{h,k}$	characteristic embedment strength (N/mm^2)
$f_{head,k}$	characteristic pull-through parameter of screw head (N/mm^2)
$f_{t,k}$	characteristic tensile strength (MPa)
$f_{v,k}$	characteristic shear strength
G	elastic shear modulus (MPa)
G_j	total dead load of storey j (N)
g	gravitational acceleration ($kg/(ms^2)$)
K_{ax}	axial stiffness
K_i	elastic stiffness along DoF i (kN/mm)
K_{IC}	inter-compartment stiffness (kN/mm)
K_{lat}	lateral stiffness
l	penetration length of thread (mm)
M_j	equivalent moving mass of storey j (kg)
M_{max}	maximum or ultimate moment (Nm)
M_y	yield moment (Nm)
$P(X)$	probability of event X
$P(X\|Y)$	probability of X, given Y
$P_j(\delta)$	pushdown curve of storey j (kN)
Q_j	total live load of storey j (N)
q_j	equivalent moving live load of storey j (N)
$R_0(t)$	force replacing the removed wall (N)
$R_j(t)$	reaction at background point of storey j (N)
S	total snow load (N)
s	equivalent moving snow load (N)
t	time (s)
$\tilde{w}_j$	vertical pressure in walls (MPa)
x_d	displacement at damage initiation (mm)
x_i	relative translation in DoF i (mm)
x_{plat}	displacement at start of plastic plateau (mm)
x_r	ultimate displacement at rupture (mm)
x_y	displacement at yield point (mm)
α	angle between screw axis and fibres (degrees)
δ	pushdown displacement (mm)

ρ_a	reference timber density (kg/m^3)
ρ_k	characteristic timber density (kg/m^3)
ρ_m	mean timber density (kg/m^3)
$\sigma_{t,0}$	tensile stresses along fibres (MPa)
$\sigma_{t,90}$	tensile stresses perpendicular to fibres (MPa)
τ_{LS}	longitudinal shear stresses (MPa)
τ_{RS}	rolling shear stresses (MPa)
$\boldsymbol{\phi}$	positioning rotation vector (degrees)
ϕ_d	rotation at damage initiation (degrees)
ϕ_i	relative rotation around DoF i (degrees)

1. Introduction

Cross-laminated timber (CLT) is used in increasing proportions for the bearing structures of multi-storey buildings. CLT is composed of cross-wise laminae of parallel timber boards and is used for wall and floor panels (Brandner, 2013). Currently, the tallest timber buildings (both 18 storeys) are Mjøstårnet in Brumunddal, Norway (Abrahamsen, 2017) and Brock Commons Tallwood House in Vancouver, Canada (Fast *et al.*, 2017), and both use CLT panels as floors. Pure CLT buildings can either be balloon-framed, with continuous walls, or platform-framed, where the floors of each storey are supported on top of the walls of the storey below, which results in across-the-grain compression in the floors and thus limits the achievable building height (Gagnon and Pirvu, 2011). The nine-storey Stadthaus in London, UK, is an example of a platform-framed CLT building (Wells, 2011).

In a multi-storey building with high occupancy, disproportionate collapse resulting from an unforeseeable event such as an accident or act of terrorism needs to be avoided as the consequences would be severe (BSI, 2006). The total probability of a disproportionate collapse, $P(C)$, is usually expressed by (Ellingwood and Dusenberry, 2005)

$$1. \quad P(C) = \underbrace{P(E)}_{\text{Exposure}} \cdot \underbrace{P(D|E)}_{\text{Vulnerability}} \cdot \underbrace{P(C|D)}_{\text{Robustness}}$$

where $P(E)$ is the probability of an unforeseen event, $P(D|E)$ is the probability of initial damage given the unforeseen event and $P(C|D)$ is the probability of disproportionate collapse given the initial damage. These terms are respectively referred to as exposure, vulnerability and robustness (Starossek and Haberland, 2010), each posing a line of defence (Ellingwood *et al.*, 2007), of which mostly vulnerability and robustness can be affected by engineering choices (Starossek and Haberland, 2010).

Compared with concrete and steel buildings, a lack of guidance has been identified concerning the design for the structural robustness of multi-storey CLT buildings (Huber *et al.*, 2019). Robustness requires the availability of alternative load paths (ALPs) that are to be activated when a part of the vertical bearing structure has been removed (Ellingwood *et al.*, 2007). Examples of ALPs include catenary action in beams, membrane action in floors and deep beam action of wall sections above removed walls (Huber *et al.*, 2019). The ability for load transfer under large deformations in the connections is essential for an ALP to function as intended (Byfield *et al.*, 2014).

An ALP analysis yields the response of a structure to an assumed component loss (Ellingwood *et al.*, 2007) and assesses how the ALPs develop; this is usually achieved by finite element analysis (FEA) to account for non-linearities and dynamic effects (Izzuddin *et al.*, 2008). Using FEA, Mpidi Bita *et al.* (2018) conducted an ALP analysis of a 12-storey platform-framed CLT building by dynamic removal of the middle support wall of a double-span floor at the ground storey. They found that the ALPs required larger capacities than those supplied by commonly used fasteners. Mpidi Bita and Tannert (2019a) conducted an ALP analysis using FEA of a nine-storey glue laminated (glulam) timber column-framed building with CLT floors by removing various columns. They found that the structure could engage in a hanging action of the floors from the remaining columns, in catenary action of the floor panels and in a horizontal tie action of the damaged bay from the remaining building core. Mpidi Bita and Tannert (2019b) presented an analytical linear elastic procedure for designing ALPs in platform-framed CLT buildings, assuming that catenary action of the floor panels, cantilever action in a damaged corner bay and deep beam action in an internal bay would develop after removal of a wall.

In the studies reported in the literature so far, ALPs have been investigated on a global building level where components and their interactions have been simplified and the mechanical behaviour of multiple fasteners in a connection has been condensed to a single point. However, a recent study by Huber *et al.* (2018) showed that modelling single fasteners between CLT components may reveal progressive rupture in a zipper-like fashion under non-uniform loading after wall removal. Furthermore, the ALPs in platform-framed CLT buildings, which – for the sake of sound insulation – consist of separated bays with single-span floors have so far not been investigated. It is assumed that, after a removal in these buildings, the compressed floor panels between the walls could result in friction and local timber crushing, governing the ALP development with varying extents at different storeys. A detailed understanding of the mechanisms governing the development of ALPs at the component level is required in order to correctly assess the behaviour of the entire building at a global level after a wall removal. The goal of this work was to address the following research questions, considering the removal of a single wall panel at the ground storey of a single-span, platform-framed CLT bay.

- What ALPs may develop on single storeys?
- How do the building components and connections contribute to the development of ALPs on single storeys?
- How is the entire bay affected after the removal?

To approach answers to these questions, FEA using the commercial software Abaqus (DS, 2014) was used, accounting for non-linearities – that is, fastener failure, frictional contact, compressive crushing, tensile failure and large displacements.

2. Method

2.1 Case building

The conducted analysis was based on an existing eight-storey platform-framed CLT building in Sweden, made of separated bays with single-span floors and balconies (see Figure 1(a)). The storey height is 3 m. For the worst case scenario, a corner bay was investigated, with simplifications for the sake of modelling (see Figure 1): (*a*) any openings in the panels were ignored; (*b*) each storey was assumed to be similar; (*c*) the shape of the floor plan of the bay was made more quadratic to obtain a generic setup and to capture a recommended wall removal length of approximately twice the storey height (Huber *et al.*, 2019); (*d*) the surrounding structure was coupled by linear springs at four locations on each storey. The surrounding spring stiffness was set to 7·4 kN/mm, which was estimated by loading the remaining structure sideways in a separate finite element (FE) model and measuring the reactions. All panels were five-ply CLT made of C24 graded timber with lap-joints between the floor panels (see Figure 2). The removal of a wall panel supporting all three floor panels at the bottom storey was studied.

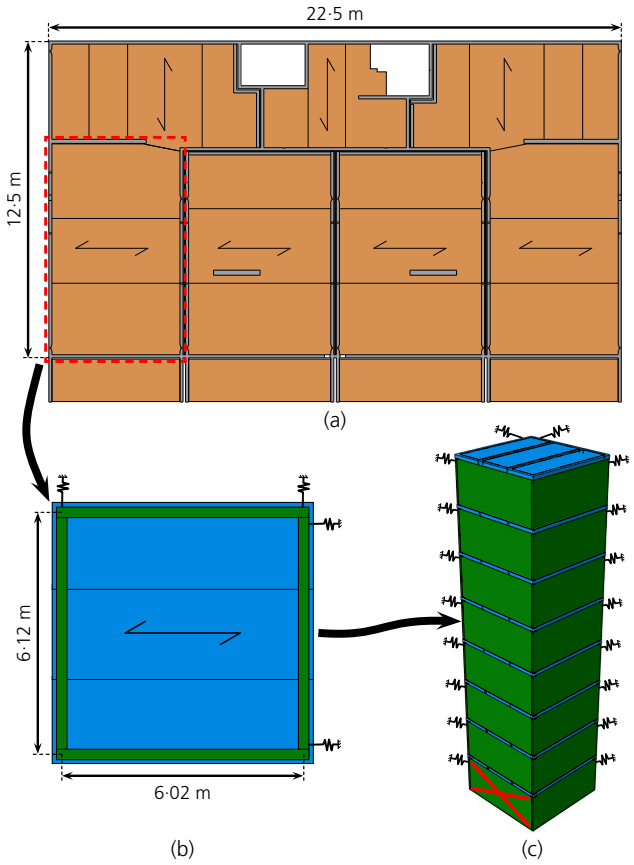

Figure 1. Studied building: (a) floor plan of the case building including balconies, with the investigated bay highlighted; (b) simplified floor plan of the investigated bay; (c) simplified model of the studied corner bay indicating the removed wall

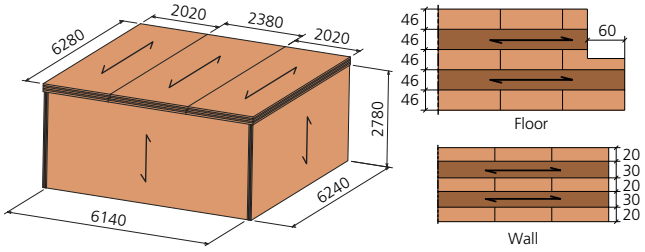

Figure 2. Specifications of the CLT panels in storeys. Dimensions in mm with dimension lines using the outer edges of the panels and the middle of the lap-joints as references

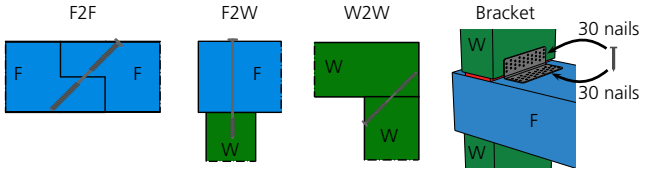

Figure 3. Fastener installations in the building: floor panels (F) are connected to wall panels (W)

Four connections exist in the structure (see Figure 3) – floor-to-floor (F2F) connections in the lap-joints, floor-to-wall (F2W) connections between the floor panels and their supporting walls, wall-to-wall (W2W) connections in the corners and angle bracket connections between the floor panels and the walls of the next storey. Between the floors and the edges of the wall panels of the next storey, a 25 mm thick rubber sound insulation exists; this was ignored in all but the simplified dynamic model (see Section 2.4). In the connections, self-tapping screws (ETA-12/0063 (Eota, 2012); ETA-12/0373 (Eota, 2017)) and angle brackets of type TTF200 (ETA-12/0496 (Eota, 2014)) are installed (see Table 1). The angle brackets are 3 mm thick and fixed with 30 ring-shanked anchor nails (see Table 1) on each flange.

2.2 FE model

The component method was used to model the connections, which has previously been successfully applied to model steel and concrete connections after removal of an element (Stoddart *et al.*, 2014; Stylianidis and Nethercot, 2015) and to evaluate timber connections under seismic loads (Fragiacomo *et al.*, 2011; Rinaldin *et al.*, 2013). The active parts of connections were substituted by their respective force–deformation behaviour to save computational cost while keeping the model sufficiently realistic. In the models, the screws and brackets were replaced by 'finite connector elements' to account for

Table 1. Specifications of fasteners in the bay

Fastener	Dimensions: mm	Centre to centre spacing: mm	Thread	Inclination: degrees
F2F	8·2 × 245	400	Single	45
F2W	6·0 × 300	400	Double	0
W2W	6·5 × 160	400	Double	45
Angle bracket	200 × 71 × 71	1000	—	—
Anchor nail	4·0 × 60	—	Ring	0

non-uniform loading and progressive rupture. Henceforth, the finite connector elements are referred to as 'connector elements', while the screws and angle brackets as referred to as 'fasteners'.

The Abaqus connector element in three-dimensional (3D) space (Conn3D2) is a two-node 1D element that defines a constitutive behaviour between the degrees of freedom (DoF) of its nodes (node a and node b) (DS, 2014). Attached to each node, the element contains a coordinate system (directions x_1, x_2 and x_3) to follow their motions. The nodes were coupled to a cloud of mesh nodes on the respective surfaces in connection. All relative motions between the nodes were measured as seen from the coordinate system of node a. The constitutive mechanical behaviour of the element was based on the relative changes in translation (δx_i) and rotation ($\delta\phi_i$), which obey Equations 2 and 3 for an arbitrary motion of node b from position b′ to b, considering large deformations.

$$\delta x_i = x_{i,\mathrm{b}} - x_{i,\mathrm{b}'} \quad (2)$$

$$\delta\phi_i = \phi_{i,\mathrm{b}} - \phi_{i,\mathrm{b}'} \quad (3)$$

Here, $x_{i,\mathrm{b}}$ and $x_{i,\mathrm{b}'}$ denote the coordinates of b and b′ respectively in system a, and $\phi_{i,\mathrm{b}}$ and $\phi_{i,\mathrm{b}'}$ denote the components of the rotation vector ($\boldsymbol{\phi}$), which positions the coordinate axes at b and b′ relative to the axes at a (DS, 2014).

The constitutive behaviour was specified for each DoF. Figure 4 shows the generic force–displacement behaviour used in this study, equivalently applied for moments, along DoF i. The elastic stiffness was K_i, optionally followed by a plastic yield point at $\{x_{i,\mathrm{y}}, F_{i,\mathrm{y}}\}$ and a subsequent hardening up to a plastic plateau at $\{x_{i,\mathrm{plat}}, F_{i,\mathrm{max}}\}$, ultimately followed by the motion-based damage initiation point at $\{x_{i,\mathrm{d}}, F_{i,\mathrm{max}}\}$. After damage initiation, the force responses along all DoFs were degraded exponentially until total failure (rupture) at $x_{i,\mathrm{r}}$. The failure motion (i.e. $x_{i,\mathrm{r}} - x_{i,\mathrm{d}}$) was set to approximately $x_{i,\mathrm{d}}/10$ to avoid abrupt stiffness changes that could jeopardise convergence.

When replacing a self-tapping screw, the screw axis was aligned with x_3 of node a, and only translational DoFs were used. For the lateral stiffness (along x_1 and x_2), K_{lat} was used from

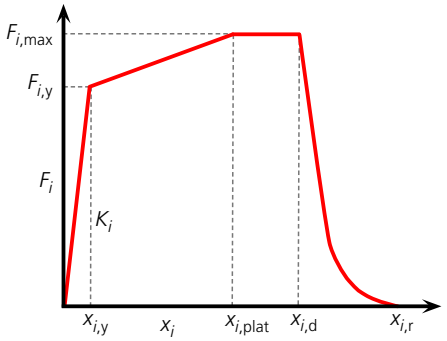

Figure 4. Generic force–displacement curve for the i-th DoF of a connector, showing elastic stiffness (K), yield point (y), plastic plateau (plat), damage initiation (d) and rupture (r)

Equation 4 (taken from BS EN 1995-1-1:2004 (BSI, 2004)). For the axial stiffness, K_{ax} from Equation 5 (taken from ETA-12/0063 (Eota, 2012) and ETA-12/0373 (Eota, 2017)) was used.

$$K_{\mathrm{lat}} = \frac{\rho_{\mathrm{m}}^{1.5}\, d}{23} \quad (4)$$

$$K_{\mathrm{ax}} = 25\, l\, d \quad (5)$$

Here, ρ_{m} is the mean timber density (in kg/m^3), d is the nominal screw diameter in mm, l is the penetration length of the screw thread in mm and K is in N/mm.

For axial screw loading, brittle behaviour was assumed (i.e. no plastic branch in Figure 4). For the W2W and F2F screws, thread extraction governed the axial strength, and $F_{\mathrm{ax,max}}$ (in N) was calculated using Equation 6 from Uibel and Blaß (2014). For the F2W screws, head pull-through governed the strength, and $F_{\mathrm{ax,max}}$ was calculated using Equation 7 from ETA-12/0373 (Eota, 2017).

$$F_{\mathrm{ax,max}} = \frac{0{\cdot}35\, d^{-0.8}\, l\, \rho_{\mathrm{k}}^{0.75}}{1{\cdot}5\cos^2\alpha + \sin^2\alpha} \quad (6)$$

$$F_{\mathrm{ax,max}} = f_{\mathrm{head,k}}\, d^2 \left(\frac{\rho_{\mathrm{k}}}{\rho_{\mathrm{a}}}\right)^{0.8} \quad (7)$$

In these equations, ρ_k is the characteristic density (in kg/m^3), α the angle between the screw axis and the fibres (in degrees) and $f_{head,k}$ is the characteristic pull-through parameter of the screw head (in N/mm^2) at the reference timber density ρ_a (in kg/m^3), $f_{head,k}$ and ρ_a given in ETA-12/0373 (Eota, 2017).

For lateral screw loading, ideal plasticity was assumed (i.e. no hardening branch in Figure 4). The yield point ($F_{lat,y}$) was calculated using Equation 8, after evaluating all six Johansen failure modes ($F_{R,a}$ to $F_{R,f}$, in N) from BS EN 1995-1-1:2004 (BSI, 2004). The Johansen modes are functions of the characteristic embedment strength of the timber ($f_{h,k}$, in N/mm^2), which was calculated according to Equation 9 from Blaß *et al.* (2006), the thickness of the connected components, the screw diameter and the characteristic screw yield moment (taken from ETA-12/0063 (Eota, 2012) and ETA-12/0373 (Eota, 2017)). Three of the failure modes additionally depend on $F_{ax,max}$ due to the roping effect (BSI, 2004).

8. $$F_{lat,y} = \min\ \{F_{R,a}, F_{R,b}, F_{R,c}, F_{R,d}, F_{R,e}, F_{R,f}\}$$

9. $$f_{h,k} = \frac{0{\cdot}019\,\rho_k^{1{\cdot}24}\,d^{-0{\cdot}3}}{2{\cdot}5\cos^2\alpha + \sin^2\alpha}$$

No interaction was modelled between the DoF in the elastic branches. However, for the yield point in the screws, a coupled criterion according to Equation 10 was assumed to ensure an equal yield point in the plane perpendicular to x_3 (i.e. a cylindrical yield surface), which follows the reasoning in BS EN 1995-1-1:2004 (BSI, 2004) for mixed load states of fasteners. Similarly, the damage initiation point was coupled between all DoFs according to Equation 11 (i.e. an ellipsoid damage surface).

10. $$\left(\frac{F_1}{F_{1,y}}\right)^2 + \left(\frac{F_2}{F_{2,y}}\right)^2 = 1$$

11. $$\left(\frac{x_1}{x_{1,d}}\right)^2 + \left(\frac{x_2}{x_{2,d}}\right)^2 + \left(\frac{x_3}{x_{3,d}}\right)^2 = 1$$

where the common value $x_{1,d} = x_{2,d} = 20$ mm was set and $x_{3,d} = F_{ax,max}/K_{ax}$.

The bracket was first studied in a separate FEA with a 2D shell model of the bracket steel, connector elements for the nails and 3D solids to represent the wooden contact areas of the flanges (see Figure 5). For the nails, the trilinear force–displacement behaviour given by Izzi *et al.* (2018) was used, who experimentally validated their modelling approach of the same bracket. The force–deformation behaviour of the bracket was recorded while moving the lower contact area in shear (x_1 in Figure 5), uplift (x_2 and x_3) and hinging rotation (ϕ_1), one at a time. The model accounted for plasticity, friction, contact and large deformations. The results were then used as input values for the connector elements substituting the brackets.

Since a 3D analysis of the entire bay at the desired level of detail was deemed to be too computationally expensive, the analysis was subdivided into three representative compartment models (see Figure 6) – one for the bottom storey, one for the

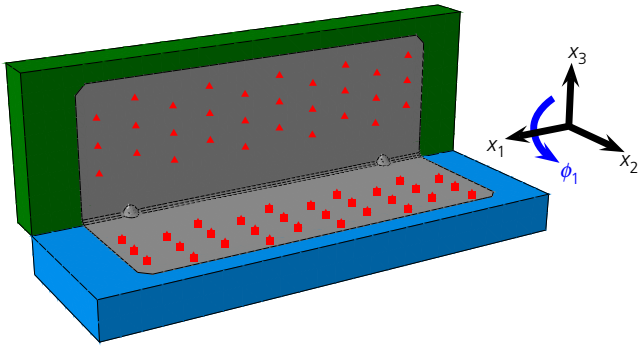

Figure 5. FE model of the angle bracket: dots showing the connector elements substituting the nails between the bracket and the support at the flanges

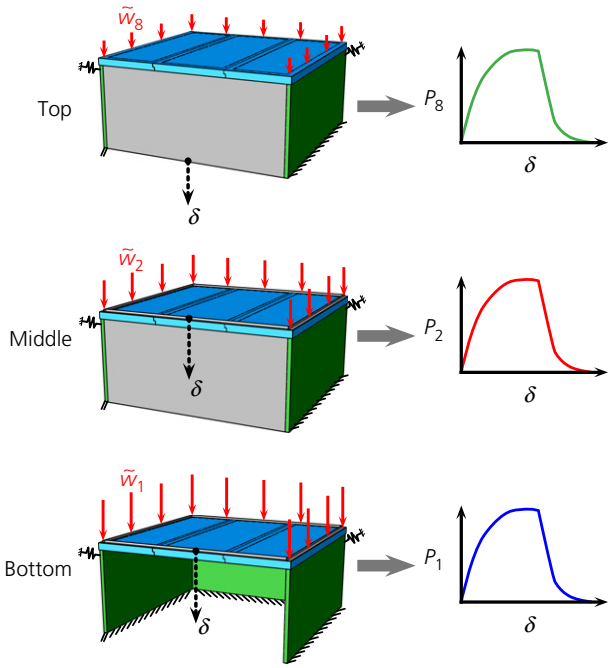

Figure 6. Analysis procedure: three compartment models at the representative storeys were analysed and their pushdown curves were established

top storey and one for the storeys in between. Each compartment included the walls of the respective storey and the floor panels supported by them. The surroundings were replaced by suitable boundary conditions and simplifications (as described in Section 2.3). The modelling of all compartments was similar; as an example, Figure 7 shows the upper quarter of the bottom compartment model. Each floor panel was modelled by an outer 'cage', finely meshed with quadratic brick elements (C3D20R), which was tied to an inner 'core', coarsely meshed with continuum shell elements (SC8R). In thickness, the cages contained two elements per CLT ply to increase the stress resolution with regard to compressive crushing, while the cores contained a single element that accounted for all CLT plies by a composite layup, enforcing shear flexible (Mindlin–Reissner) plate theory (DS, 2014). The walls below were modelled in a similar way to the cores and the walls of the next storey were simplified by L-shaped rigid surfaces since the vertical deflection of these walls was estimated to be small compared with that of the floor panels. The L-shape provided both a horizontal contact surface for the vertical loads and a vertical surface that the connector elements substituting the brackets could be coupled to. The surrounding structure beyond the bay was modelled as rigid in the background around the compartment. The connector elements were inserted at the fastener locations between the connected parts and at the locations of the stiffness between the surrounding structure and the bay (see Figure 7(b)).

Material data for timber grade C24 based on characteristic strengths were used for all components according to Table 2, with Poisson's ratios set to zero. An orthotropic linear elastic material model was applied for all the flexible components. For the floor cages, additionally an ideal-plastic material model was used to account for compressive timber crushing,

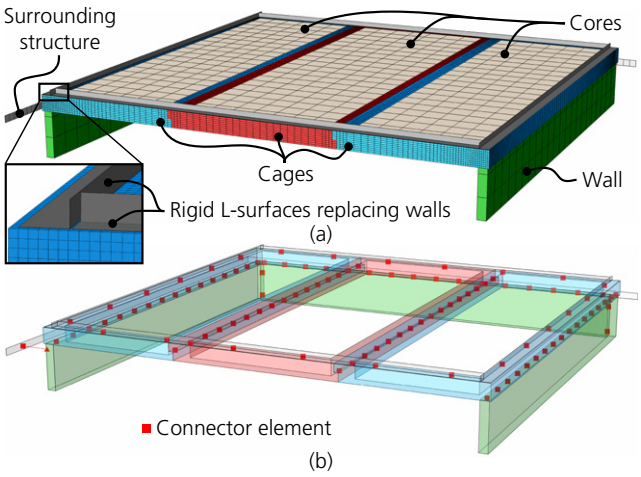

Figure 7. Modelling details exemplified for the upper quarter of the bottom compartment: (a) meshed view of the walls and floors; (b) translucent view, with connector elements shown as squares

Table 2. Linear elastic modulus, shear elastic modulus (G) and characteristic strengths (f_k) in tension, compression and shear for C24 graded timber (from BS EN 338:2016 (BSI, 2016))

	Elastic modulus: MPa	G: MPa	$f_{t,k}$: MPa	$f_{c,k}$: MPa	$f_{v,k}$: MPa
Along fibres (0°)	11 000		14·5	21·0	
Across fibres (90°)	370		0·4	2·5	
Longitudinal shear		690			4·0
Rolling shear		50			1·0

which was based on a Tsai–Wu yield surface (Tsai and Wu, 1971) by implementing an Abaqus subroutine presented by Ekevad (2006). The uniaxial yield points were set to the strength values in Table 2. Furthermore, brittle failure in only tension and shear was tracked in the subroutine by applying a maximum stress criterion according to

$$\max\left\{\frac{\sigma_{t,0}}{f_{t,0,k}}, \frac{\sigma_{t,90}}{f_{t,90,k}}, \frac{\tau_{LS}}{f_{v,LS,k}}, \frac{\tau_{RS}}{f_{v,RS,k}}\right\} \geq 1 \quad (12)$$

where σ_t and τ are the tensile and shear stresses, respectively and subscripts 0 and 90 denote the angle to the fibre direction and LS and RS denote longitudinal and rolling shear, respectively. Between all the components, normal contact was modelled with a 'hard' pressure–overclosure law, where arbitrarily large contact stresses could occur to prohibit penetration (DS, 2014), and tangential friction was modelled with an isotropic coefficient of 0·3.

2.3 ALP analysis of single storeys

To elicit the ALPs, a pushdown analysis was conducted, during which the section above the removed wall was pushed down quasi-statically until ultimate failure occurred and the respective force–displacement response (i.e. the pushdown curve) was recorded (Izzuddin *et al.*, 2008; Khandelwal and El-Tawil, 2011). Separate analyses were conducted on the three compartment models (see Figure 6), with the assumption that the behaviour of the entire bay could be described by combining the behaviour of the single compartments in a later step. In the bottom compartment, the removed wall was not modelled and a gap existed instead. Each compartment model thus contained at least three walls, henceforth called 'stationary walls', in vertical alignment with the remaining walls on the bottom storey. The middle and top compartments additionally contained a wall that was assumed to move downwards, above the gap. The stationary walls of each compartment model were rigidly fixed at their bottom as a first approximation of their rather stiff connection by angle brackets to the floor below, which was not modelled. The bottom movement of the stationary walls was considered less significant for the analyses because most movement was expected in the floor panels. The moving walls were unrestrained by external boundary conditions. In the bottom

and middle compartments, the pushdown was performed by moving down the rigid L-surface above the gap in a deformation-controlled manner; for the top compartment, the bottom of the moving wall was pulled down instead.

Before the pushdown was started, vertical loads $\tilde{w}_j$ were applied as pressures on the rigid L-surfaces for the bottom and middle compartment and on a corresponding surface on the outer edges of the roof panels for the top compartment. For simplification, no floor and snow loads were applied; instead, their contribution was accounted for in $\tilde{w}_j$. For storey j, $\tilde{w}_j$ was calculated according to Equation 13, which corresponds to the accidental load combination required for ALP analyses in BS EN 1990:2002 (BSI, 2002).

$$\tilde{w}_j = \frac{1}{A}\left(0{\cdot}2S + \sum_{m=j}^{8}(G_m + 0{\cdot}5Q_m)\right) \quad 13.$$

In Equation 13, G_j and Q_j are, respectively, the total dead and live loads (in N) of storey j, S is the total snow load (in N) and A is the total horizontal cross-sectional surface of four wall panels (in m^2). It was assumed that the four walls of a compartment carried the loads equally before the removal. For the middle compartment, the loads of the storey directly above the removed wall ($j = 2$) were used. Large deformations were accounted for and a quasi-static implicit dynamic calculation regime using the backward Euler integrator was applied to increase convergence (DS, 2014).

Lacking experimental data, a manual criterion was introduced (see Figure 8) to evaluate whether brittle shear failure would occur in the floor panels above the support; only the strongest plies regarding transverse shear were considered (i.e. ply 2 and ply 4), which were loaded in longitudinal shear. The elements marked as failed by the maximum stress criterion in the finely meshed cages were projected onto a cross-section above the support walls. The criterion was met when, in the projection, the cross-section of one ply was entirely marked as failed. Thereafter, any load transfer by way of the cross-section of the floor panels was considered to be inhibited in the models. The assumption behind the criterion was that a crack could propagate along the ply if, in the projection, the entire ply was marked as failed.

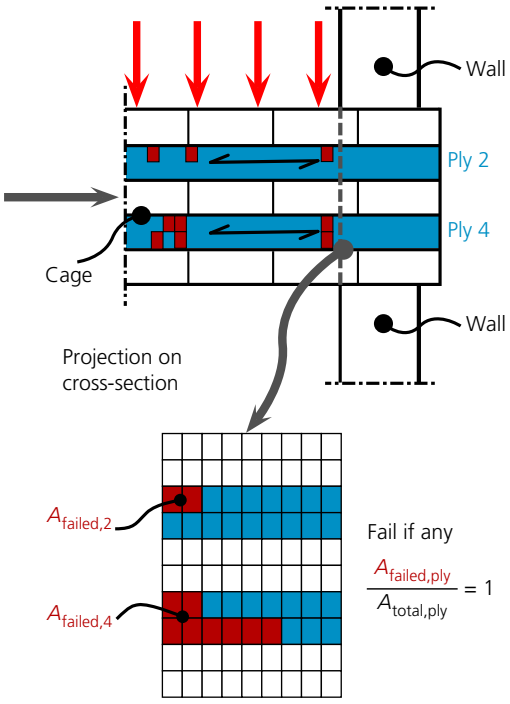

Figure 8. Tensile failure criterion: if the projection of the failed elements in ply 1 or 2 of the floor cages filled the cross-section of one ply, brittle failure was assumed

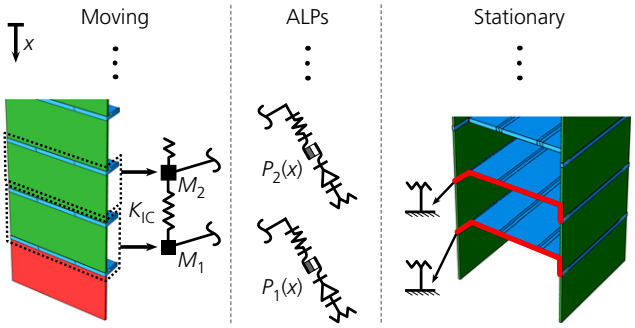

Figure 9. Simplifications for the dynamic model: moving masses were condensed to points, aggregated ALPs were substituted by a connector element at each storey and the stationary parts were simplified by fixed supports

2.4 Non-linear dynamic analysis of the entire bay

The pushdown curves (P_j) elicited during the ALP analysis were subsequently used to substitute the force–displacement behaviour of the respective storeys in a simplified dynamic model of the entire bay (see Figure 9). Those parts of the storeys that were assumed to be moving were condensed to point masses (M_j), which were interlinked by an inter-compartment stiffness (K_{IC}), and those parts that were assumed to remain stationary were substituted by a fixed background point at each storey. K_{IC} was calculated by assuming a parallel action of the stiffness of the angle brackets and the sound insulation along the wall edges. Each point mass was coupled to its background point by a connector element that substituted the elastic, plastic and damage behaviour of the pushdown curve (i.e. the aggregated behaviour of the ALPs) of the respective storey.

The reassembled dynamic model is shown in Figure 10; the system could only move vertically (along x) subjected to gravitational acceleration $\boldsymbol{g}$, the time-dependent force $R_0(t)$ substituted the wall to be removed and the equivalent shares of the live load (q_j) and the snow load (s) were applied as point loads. It was assumed that only the moving walls and a quarter of the floor weight would contribute to the moving

masses, which resulted in $M_j = 0{\cdot}25\ G_j/\boldsymbol{g}$, and, correspondingly, $q_j = 0{\cdot}5\ Q_j/4$ and $s = 0{\cdot}2\ S/4$. $R_0(t)$ kept the system in static equilibrium at $t = 0$ and was subsequently reduced to zero along a sigmoid curve over the removal time. Following a recommendation of the US Department of Defense (US DoD, 2016), the removal time was set to slightly less than one tenth of the period of the first vertical eigenmode of the compartment models. The eigenmodes were evaluated by modal analyses in the FE software and the shortest period among the compartments was used. The forces directed to ground at the respective background points, $R_j(t)$, were recorded. An implicit dynamic calculation regime using the Hilber–Hughes–Taylor integrator with the default transient fidelity settings (DS, 2014) was applied to capture the transient response.

3. Results

3.1 Fasteners

The input values for the connector elements of all the fasteners are shown in Table 3. For translational movement of the bracket, the stiffness values in Table 3 were based on the simulations; however, the yield and ultimate strength values (66·5 kN in shear and 50 kN in uplift) were approximations to the results reported by Izzi *et al.* (2018). All rotational results were based on the simulations. The bracket behaved differently in opening and closing rotations (see Figure 11) mainly because, during closing, the flanges were fully supported by the contacting surfaces whereas, during opening, the flanges were only supported by the nails. Nevertheless, in the connector elements, the hardening behaviour was simplified by averaged values to facilitate implementation.

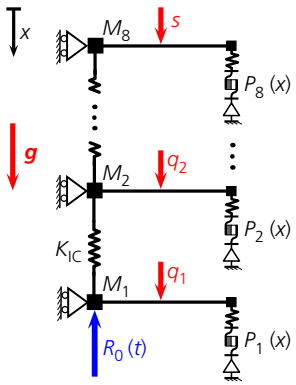

Figure 10. Simplified non-linear dynamic model, showing point masses M_j, equivalent live loads q_j, equivalent snow loads s, inter-compartment stiffness K_{IC}, the force replacing the removed wall $R_0(t)$ and the inserted ALP behaviours $P_j(x)$ of each compartment

3.2 ALPs

Four different ALPs were identified in the compartment models. Figure 12 shows a schematic illustration of the ALPs in each compartment model.

- ALP I – a shearing action in the outer floor panels, transferring loads from the pushing wall from above to the supporting stationary walls below. This ALP was limited by transversal shear failure in the floor panels due to the load concentrations beneath the pushing wall.
- ALP II – an arching action of the moving wall, transferring loads to the stationary walls by way of the W2W connectors. This ALP was limited by the capacity of the W2W connectors.
- ALP III – a mechanism resembling catenary action between the floor panels, transferring loads by way of various connectors and friction horizontally. This ALP was predominantly sustained by the tensile capacity of the F2F joints.
- ALP IV – a hanging action from the roof panels, transferring loads by way of the W2F screws to the roof. This ALP was limited by the rip-out capacity of the W2F screws.

ALP II could not occur in the bottom compartment because it lacked a moving wall and, naturally, ALP IV could only occur in the top compartment. The contributions of different components to the ALPs in the compartments were estimated from measurements in the FE models at the maximum load state for each ALP (a summary is provided in Table 4). For all the compartments, ALP III provoked non-uniform loading of the F2F screws along the lap-joints, with the screws closest to the moving wall taking the highest loads and the screws

Table 3. Connector element input data

Translations						Rotations					
		K: kN/mm	F_y: kN	F_{max}: kN	x_d: mm			K: Nm/degree	M_y: Nm	M_{max}: Nm	ϕ_d: degrees
F2F	Lateral	3·07	4·51	4·51	20·00	Bracket	Closing	91·6	154	600	45
F2F	Axial	21·94	—	8·20	0·37	Bracket	Opening	63·0	154	600	45
F2W	Lateral	2·25	1·41	1·41	20·00						
F2W	Axial	9·60	—	2·10	0·16						
W2W	Lateral	2·43	2·02	2·02	20·00						
W2W	Axial	10·56	—	4·34	0·41						
Bracket	Shear	6·71	66·5	66·5	20·00						
Bracket	Uplift	3·77	50·0	50·0	20·00						

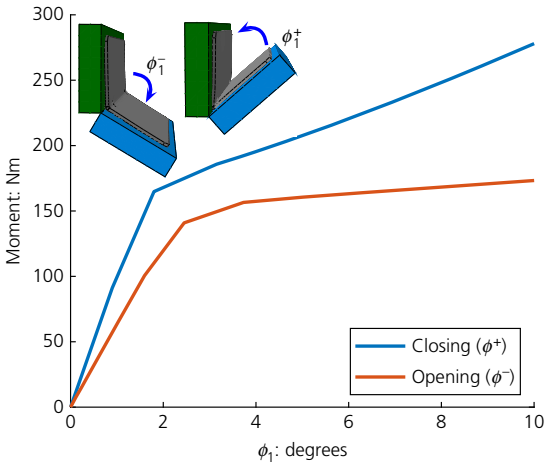

Figure 11. Simulated bracket behaviour in hinging rotation. A full-colour version of this figure can be found on the ICE Virtual Library (www.icevirtuallibrary.com)

furthest away being barely loaded. However, loading of the F2F screws never exceeded 50% of their capacity.

The corresponding pushdown curves for the various compartment models are shown in Figure 13. The bottom and middle compartments both exhibited a non-linear hardening response up to approximately 7 mm of pushdown displacement, which was primarily a result of compressive timber crushing as a result of ALP I. At larger displacements, the shear failure criterion was met and the loads along ALP I and ALP III dropped to zero. In the middle compartment, only ALP II could subsequently transfer loads until itself was ultimately exhausted at 20 mm of displacement (i.e. when the W2W screws failed). The top compartment exhibited a linear response up to approximately 1·5 mm of displacement, which was predominantly carried by ALP II (here in the flipped direction; see Figure 12(a)). At larger displacements, the rotation of the floor panels led to non-uniform loading of the W2F screws, resulting in a zipper-like progressive rip-out of all the W2F screws, which was completed at approximately 9 mm displacement (see the magnified inset in Figure 13). Subsequently, only ALP II transferred the loads, until ultimate failure occurred.

A cut through the load situation at the load concentration above the gap, beneath the pushing L-surface, can be seen in Figure 14. The top layer of the floor cage crushed locally (i.e. deformed plastically) in the region of edge contact with the pushing L-surface above and to the stationary wall below. The crushing remained local because the stresses could distribute in the deeper layers of the cross-section. As the pushdown movement of the L-surface proceeded, it provoked a rotation of the floor panel and subsequently an outwards movement of the supporting wall, resulting in a reaction force of the spring towards the surrounding structure, normal and frictional reactions in the walls, reactions in the fasteners and friction between the

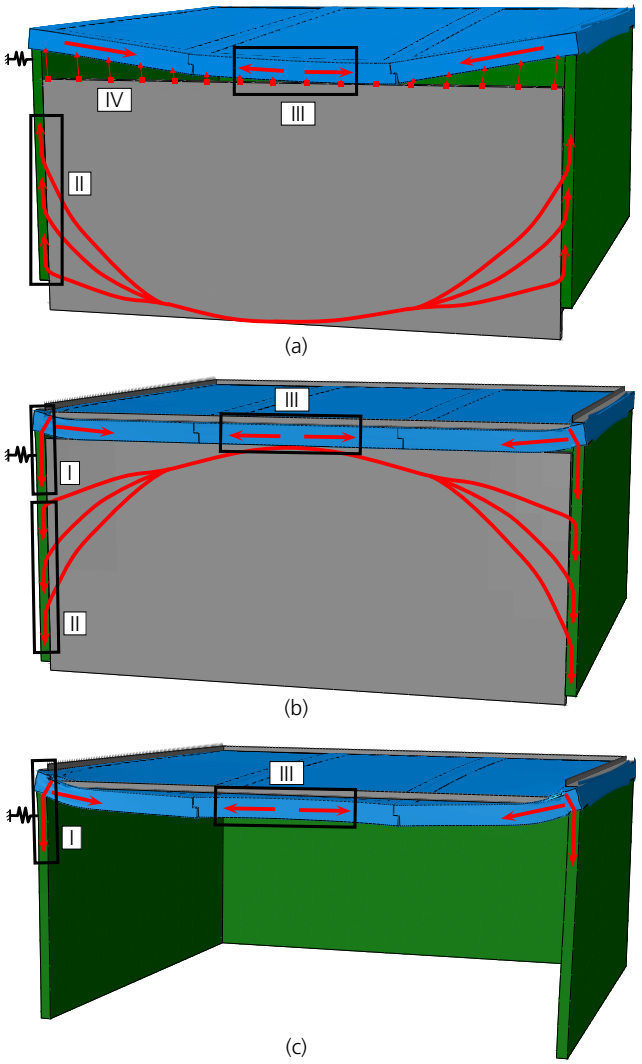

Figure 12. ALPs under pushdown: (a) top compartment; (b) middle compartment; (c) bottom compartment. The deformations are approximately 20 times magnified

Table 4. Estimated contributions to the ALPs

	Occurring in	Contributors to ALP	
ALP I	Bottom and middle	100%	Transverse panel shear
ALP II	Middle and top	100%	W2W screws
ALP III	Bottom	91%	F2F screws
		9%	Brackets
	Middle	54%	F2F screws
		26%	Friction
		15%	W2F screws
		5%	W2F screws
	Top	100%	F2F screws
ALP IV	Top	100%	W2F screws

L-surface and the floor panel. Spring, friction and normal forces contributed the most, and the fasteners contributed only negligibly to the force balance at the shown location.

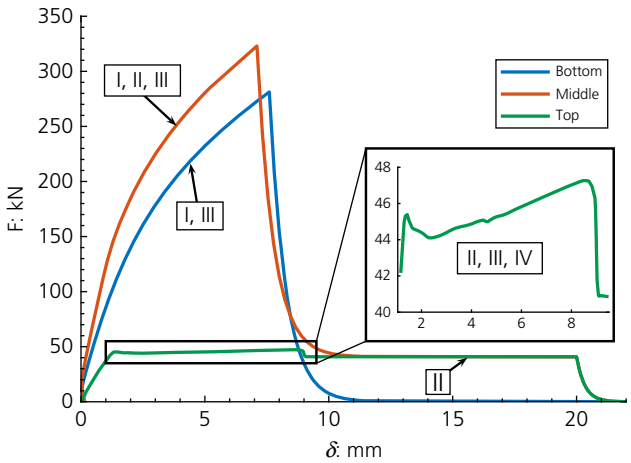

Figure 13. Pushdown curves for various compartment models: the active ALPs are indicated and the inset on the right-hand side shows a magnification of the response of the top compartment. A full-colour version of this figure can be found on the ICE Virtual Library (www.icevirtuallibrary.com)

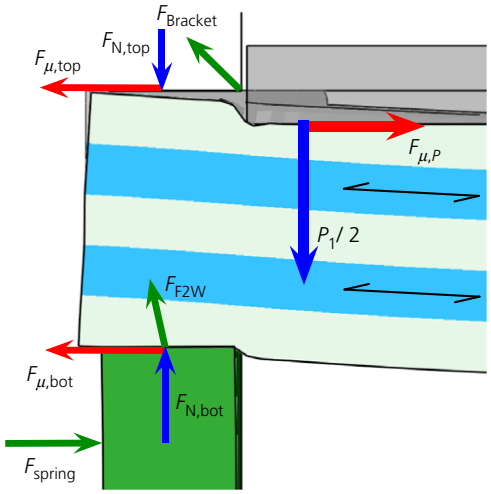

Figure 14. Cut at the load concentration above the gap in the bottom compartment, showing normal forces F_N, frictional forces F_μ, fastener forces F_{F2W} and $F_{Bracket}$, the spring force towards the surrounding structure F_{spring} and the pushdown force P_1. The deformation was magnified three times

3.3 Non-linear dynamic analysis

The removal time was 0·0078 s and $K_{IC} = 320$ kN/mm. The reactions R_j at the fixed background points for each storey are shown in Figure 15(a); the system started to oscillate without collapse after approximately 15 ms, with the loads being higher at the lower storeys. As no damping was applied, the oscillations continued indefinitely, including resonance effects among the storeys and load reversals. However, since a fully undampened system is unrealistic, only the values close to the initial peak reactions should be interpreted. Figure 15(b) shows R_j for $10K_{IC}$ rather than K_{IC} (Figure 15(a)). In this case, more load-sharing among storeys occurred compared with the original case because the dead time between the peak reactions was reduced. The first peak reaction was lower for storeys one to five, and higher for the remaining storeys. Figure 15(c) shows R_j for $K_{IC}/20$ rather than K_{IC}. This extreme case resulted in such a long dead time between the peak reactions that the ALPs exhausted sequentially from the bottom storey to the top; in other words, progressive collapse occurred. Values between K_{IC} and $K_{IC}/20$ did not result in a bay collapse.

4. Discussion

Separate ALP analyses were conducted for three representative storeys in the studied bay by means of quasi-static pushdown analyses that accounted for single fasteners, friction, timber crushing, brittle failure and geometric non-linearities. The force–displacement behaviours elicited under the ALP analyses were then inserted in a simplified dynamic model to evaluate the transient response of the entire bay.

ALP I led to a concentration of transverse shear loads above the removed wall and the corresponding strength of the floor panels limited the ultimate load along this ALP. However, the true capacity of this ALP remains uncertain because an unvalidated – yet in the authors' opinion conservative – failure criterion was used. Nevertheless, the load concentration is regarded as disadvantageous as it could provoke a brittle shear failure depending on the load redistribution capability inside the CLT. The vertical alignment of the wall joints provoked this load concentration and it seems that it could be mitigated by avoiding the repetitive pattern of isolated bays and instead shifting the wall panels horizontally at various storeys – for example, like bricks in a masonry wall. ALP II limited the arching action of the moving walls due to yielding of the W2W screws; the arching could be exploited to a greater extent by using stiffer and stronger W2W fasteners (e.g. angle brackets). ALP III provided support for ALP I and ALP IV: a failure would let the floor panels rotate and sag downwards. ALP IV was impaired by progressive rip-out of the W2F screws due to the rotation of the roof panels. Stiffening of the roof (e.g. by an additional beam) in combination with stronger fasteners may exploit this ALP to a greater extent (compare with the improved roof design proposed by Mpidi Bita and Tannert (2019a)).

The dynamic analysis showed that collapse is unlikely in the studied bay with the assumed value for the inter-storey stiffness K_{IC}. Load-sharing among the storeys increased for a high value of K_{IC} but decreased for a low value, enabling progressive collapse. K_{IC} was estimated by hand calculation and this remains to be investigated more thoroughly; nevertheless, to pose a serious threat, at least a twenty-fold reduction in K_{IC}would be required. The omission of damping in the dynamic model may be unrealistic, but this approximation seemed sufficient to study the first peak reactions at each storey and, furthermore, the results can be regarded as more conservative because damping

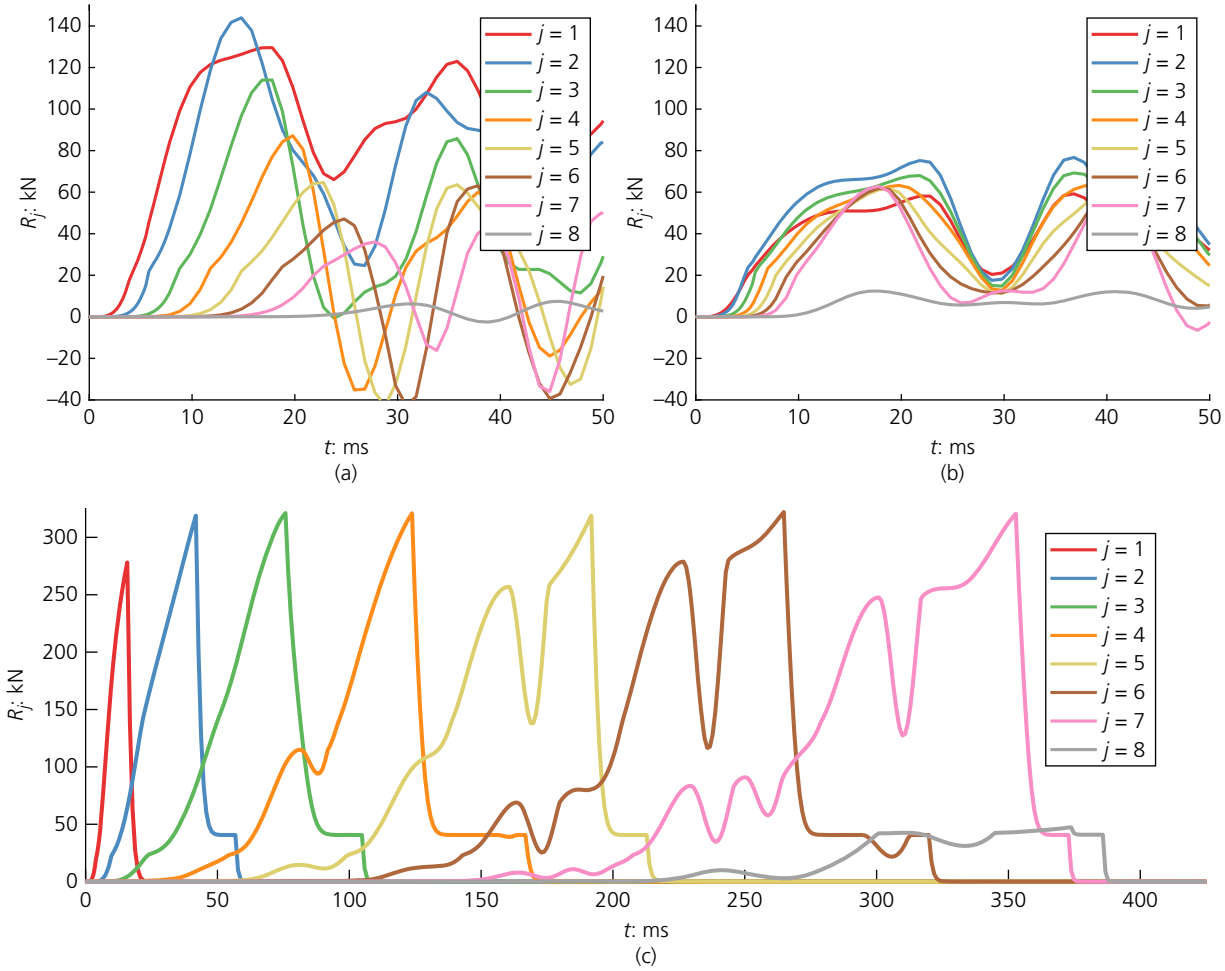

Figure 15. Dynamic response at background points for varying values of inter-compartment stiffness: (a) K_{IC}; (b) $10K_{IC}$; (c) $K_{IC}/20$. A full-colour version of this figure can be found on the ICE Virtual Library (www.icevirtuallibrary.com)

would lower the peaks. An estimation of damping and further variations of the variables may be necessary to improve the dynamic model.

Experimental investigations are necessary for validation of the model and the details of this study are contingent to the specific case building. Nevertheless, the mechanisms governing ALPs in a single-span platform-framed CLT building were studied in general, contributing to the sparse knowledge in this field and providing valuable information for structural engineers to design safer platform-framed CLT buildings. CLT buildings may offer a sustainable choice when facing the challenges of climate change regarding the housing demands of the future.

5. Conclusions

For the studied model of the bay, it was found that

- ALP I was a transverse shear action in the floor panels, ultimately limited by shear failure in the CLT
- ALP II supported an arching (deep beam) action of the walls, limited by the lateral capacity of the W2W fasteners
- ALP III supported a catenary action in the floor panels, predominantly governed by the capacity of the F2F fasteners
- ALP IV supported a hanging action from the roof, limited by the axial capacity of the W2F fasteners
- the bay could sustain a dynamic single wall removal on the bottom storey without collapsing.

However, as already noted, experimental validations are required in the future, specifically for the failure mode under the shear concentration of ALP I.

Acknowledgement

The authors thank the Vinnova BioInnovation project for funding of this work.

REFERENCES

Abrahamsen R (2017) Mjøstårnet – construction of an 81 m tall timber building. *Proceedings of the 23rd Internationales Holzbau-Forum (IHF 2017), Garmisch-Partenkirchen, Germany*. FORUM HOLZBAU, Biel/Bienne, Switzerland, pp. 1–13.

Blaß HJ, Bejtka I and Uibel T (2006) *Tragfähigkeit von Verbindungen mit selbst bohrenden Holzschrauben mit Vollgewinde*. University of Karlsruhe, Karlsruhe, Germany (in German).

Brandner R (2013) Production and technology of cross laminated timber (CLT): a state-of-the-art report. *Focus Solid Timber Solutions – Proceedings of European Conference on Cross Laminated Timber (CLT) Graz, Austria* (Harris R, Ringhofer A and Schickhofer G (eds)). University of Bath, Bath, UK, pp. 3–36.

BSI (2002) BS EN 1990:2002: Basis of structural design. BSI, London, UK.

BSI (2004) BS EN 1995-1-1:2004: Eurocode 5: Design of timber structures. General. Common rules and rules for buildings. BSI, London, UK.

BSI (2006) BS EN 1991-1-7:2006: Eurocode 1: Actions on structures. General actions. Accidental actions. BSI, London, UK.

BSI (2016) BS EN 338:2016: Structural timber. Strength classes. BSI, London, UK.

Byfield M, Mudalige W, Morison C and Stoddart E (2014) A review of progressive collapse research and regulations. *Proceedings of the Institution of Civil Engineers – Structures and Buildings* **167(8)**: 447–456, https://doi.org/10.1680/stbu.12.00023.

DS (Dassault Systèmes) (2014) *ABAQUS 6.14 Documentation*. DS, Providence, RI, USA.

Ekevad M (2006) *Modelling of Dynamic and Quasistatic Events with Special Focus on Wood-Drying Distortions*. PhD thesis, Luleå University of Technology, Luleå, Sweden. See http://ltu.diva-portal.org/smash/get/diva2:998982/FULLTEXT01.pdf (accessed 09/12/2019).

Ellingwood BR and Dusenberry DO (2005) Building design for abnormal loads and progressive collapse. *Computer-Aided Civil and Infrastructure Engineering* **20(3)**: 194–205, https://doi.org/10.1111/j.1467-8667.2005.00387.x.

Ellingwood BR, Smilowitz R, Dusenberry DO *et al.* (2007) *Best Practices for Reducing the Potential for Progressive Collapse in Buildings*. National Institute of Standards and Technology, Gaithersburg, MD, USA.

Eota (European Organisation for Technical Assessment) (2012) *European Technical Approval ETA-12/0063*. Eota, Brussels, Belgium.

Eota (2014) *European Technical Approval ETA-12/0496*. Eota, Brussels, Belgium.

Eota (2017) *European Technical Assessment ETA-12/0373*. Eota, Brussels, Belgium.

Fast P, Gafner B and Jackson R (2017) Eighteen storey hybrid mass timber student residence at the University of British Columbia. *Structural Engineering International* **27(1)**: 44–48.

Fragiacomo M, Dujic B and Sustersic I (2011) Elastic and ductile design of multi-storey crosslam massive wooden buildings under seismic actions. *Engineering Structures* **33(11)**: 3043–3053, https://doi.org/10.1016/j.engstruct.2011.05.020.

Gagnon S and Pirvu C (eds) (2011) *CLT Handbook: Cross-Laminated Timber*, Canadian edn. FPInnovations, Québec, QC, Canada.

Huber JAJ, Ekevad M, Girhammar UA and Berg S (2018) Assessment of connections in cross-laminated timber buildings regarding structural robustness. *Proceedings of 2018 World Conference on Timber Engineering (WCTE 2018), Seoul, Republic of Korea*. World Conference on Timber Engineering (WCTE), pp. 1–10.

Huber JAJ, Ekevad M, Girhammar UA and Berg S (2019) Structural robustness and timber buildings – a review. *Wood Material Science & Engineering* **14(2)**: 107–128, https://doi.org/10.1080/17480272.2018.1446052.

Izzi M, Polastri A and Fragiacomo M (2018) Modelling the mechanical behaviour of typical wall-to-floor connection systems for cross-laminated timber structures. *Engineering Structures* **162**: 270–282, https://doi.org/10.1016/j.engstruct.2018.02.045.

Izzuddin BA, Vlassis A, Elghazouli AY and Nethercot DA (2008) Progressive collapse of multi-storey buildings due to sudden column loss – Part I: simplified assessment framework. *Engineering Structures* **30(5)**: 1308–1318, https://doi.org/10.1016/j.engstruct.2007.07.011.

Khandelwal K and El-Tawil S (2011) Pushdown resistance as a measure of robustness in progressive collapse analysis. *Engineering Structures* **33(9)**: 2653–2661, https://doi.org/10.1016/j.engstruct.2011.05.013.

Mpidi Bita H and Tannert T (2019a) Disproportionate collapse prevention analysis for a mid-rise flat-plate cross-laminated timber building. *Engineering Structures* **178**: 460–471, https://doi.org/10.1016/j.engstruct.2018.10.048.

Mpidi Bita H and Tannert T (2019b) Tie-force procedure for disproportionate collapse prevention for CLT platform-type construction. *Engineering Structures* **189**: 195–205, https://doi.org/10.1016/j.engstruct.2019.03.074.

Mpidi Bita H, Currie N and Tannert T (2018) Disproportionate collapse analysis of mid-rise cross-laminated timber buildings. *Structure and Infrastructure Engineering* **14(11)**: 1547–1560, https://doi.org/10.1080/15732479.2018.1456553.

Rinaldin G, Amadio C and Fragiacomo M (2013) A component approach for the hysteretic behaviour of connections in cross-laminated wooden structures. *Earthquake Engineering & Structural Dynamics* **42(13)**: 2023–2042, https://doi.org/10.1002/eqe.2310.

Starossek U and Haberland M (2010) Disproportionate collapse: terminology and procedures. *Journal of Performance of Constructed Facilities* **24(6)**: 519–528, https://doi.org/10.1061/(ASCE)CF.1943-5509.0000138.

Stoddart EP, Byfield MP and Tyas A (2014) Blast modeling of steel frames with simple connections. *Journal of Structural Engineering* **140(1)**: 04013027, https://doi.org/10.1061/(ASCE)ST.1943-541X.0000778.

Stylianidis P and Nethercot D (2015) Modelling of connection behaviour for progressive collapse analysis. *Journal of Constructional Steel Research* **113**: 169–184, https://doi.org/10.1016/j.jcsr.2015.06.008.

Tsai SW and Wu EM (1971) A general theory of strength for anisotropic materials. *Journal of Composite Materials* **5(1)**: 58–80, https://doi.org/10.1177/002199837100500106.

Uibel T and Blaß HJ (2014) Joints with dowel type fasteners in CLT structures test material. *Focus Solid Timber Solutions – Proceedings of European Conference on Cross Laminated Timber (CLT), Graz, Austria* (Harris R, Ringhofer A and Schickhofer G (eds)). University of Bath, Bath, UK, pp. 119–134.

US DoD (US Department of Defense) (2016) *Unified Facilities Criteria (UFC) – Design of Buildings to Resist Progressive Collapse*. US DoD, Arlington, VA, USA. See https://www.wbdg.org/FFC/DOD/UFC/ufc_4_023_03_200 (accessed 09/12/2019).

Wells M (2011) Tall timber buildings: applications of solid timber construction in multistory buildings. *Council on Tall Buildings and Urban Habitat Journal* **2011(I)**: 24–27.